

# A Double-Thermostad Warm-Core Ring of the Gulf Stream

IGOR BELKIN

*College of Marine Science and Technology, Zhejiang Ocean University, Zhoushan, China, and Graduate School of Oceanography, University of Rhode Island, Narragansett, Rhode Island*

ANNIE FOPPERT

*Centre for Southern Hemisphere Oceans Research, and CSIRO Oceans and Atmosphere, Hobart, Tasmania, Australia*

TOM ROSSBY, SANDRA FONTANA, AND CHRIS KINCAID

*Graduate School of Oceanography, University of Rhode Island, Narragansett, Rhode Island*

(Manuscript received 5 February 2019, in final form 13 November 2019)

## ABSTRACT

An unusual *double-thermostad* warm-core ring of the Gulf Stream was discovered in the Slope Sea, south of Georges Bank, during the R/V *Endeavor* cruise 578 in May 2016. The ring's stratification was peculiar as it included *two* thermostads at, respectively, 100–200 m (core  $T = 18.14^{\circ}\text{C}$ ,  $S = 36.52$ ) and 250–500 m (core  $T = 16.70^{\circ}\text{C}$ ,  $S = 36.35$ ). Extensive use of satellite data (SST imagery and SSH maps) allowed the life history of this ring to be reconstructed, with independent SST and SSH data mutually corroborating each other. The double-thermostad ring was formed by vertical alignment of two preexisting warm-core anticyclonic rings of the Gulf Stream. The first ring spawned by the Gulf Stream in February has cooled by  $\sim 2^{\circ}\text{C}$  before merging in April with the second ring spawned by the Gulf Stream in March. During vertical alignment of these rings, the warmer ring overrode the colder ring, thereby forming the double-thermostad ring surveyed in May 2016. From ADCP sections through the ring, the upper and lower thermostads had different core relative vorticities of  $-0.65f$  and  $-0.77f$ , respectively, where  $f$  is the local Coriolis parameter. An in-depth literature survey has confirmed that this is the first report of a double-thermostad warm-core ring of the Gulf Stream and one of the best-documented cases of vertical alignment of two eddies ever observed in the World Ocean.


## 1. Introduction

During a short technology-testing cruise to Georges Bank southeast of Cape Cod in May 2016, a sequence of cloud-free high-resolution satellite images of sea surface temperature (SST) revealed a very well-formed warm-core ring (WCR or ring hereafter) immediately to our south. Having just completed the setup phase of our cruise, and given the proximity of the WCR, we decided

to execute a rapid XBT/CTD/ADCP ring survey. The combination of remote sensing information (SST) and XBT/CTD/ADCP instrumentation enabled us to quickly document the ring's structure and kinematics. Successive SST images allowed the ring's movement to be extrapolated so that the first XBT section targeted the ring's center, revealing *two* well-defined vertically aligned thermostads instead of a classical single thermostad of winter-cooled  $18^{\circ}\text{C}$  Water, which is a hallmark of WCRs of the Gulf Stream. This double-layer structure showed up clearly in temperature, salinity, density, and velocity. To our best knowledge, such double-thermostad WCRs of the Gulf Stream have never been reported before.

This paper starts with a brief background on double-thermostad eddies and their formation mechanisms (section 2; much more in section 6). Section 3 presents observational tools and data used in this study. Section 4 gives a detailed description of the ring from density

---

 Denotes content that is immediately available upon publication as open access.

---

 Supplemental information related to this paper is available at the Journals Online website: <https://doi.org/10.1175/JPO-D-18-0275.s1>.

---

*Corresponding author:* Dr. Igor M. Belkin, [igormbelkin@gmail.com](mailto:igormbelkin@gmail.com)

DOI: 10.1175/JPO-D-18-0275.1

© 2020 American Meteorological Society. For information regarding reuse of this content and general copyright information, consult the [AMS Copyright Policy](#) ([www.ametsoc.org/PUBSReuseLicenses](http://www.ametsoc.org/PUBSReuseLicenses)).

and velocity data. Section 5 presents the ring's life history reconstructed from remote sensing data (infrared radiometry and satellite altimetry) covering 12 months from August 2015 through July 2016. Section 6 presents various formation mechanisms of double-thermostad eddies and reviews observations of such eddies in the World Ocean. Section 7 sums up main results of this study.

## 2. Brief background on double-thermostad eddies

Double-thermostad eddies (DTE; also called double-core eddies), were identified by Kostianoy and Belkin (1989) during a global survey of lens-like subsurface eddies (Belkin et al. 1986) termed intrathermocline eddies (ITE; Dugan et al. 1982) or submesoscale coherent vortices (SCV; McWilliams 1985, 2016). A typical ITE features a single subsurface thermostad, while a DTE has two thermostads stacked up. The DTEs comprise a separate class of eddies, overlapping with the ITEs: if a DTE's upper thermostad is a subsurface one, this DTE is a two-layer (or double-core) ITE. Otherwise, if the upper thermostad outcrops, the DTE is no longer an ITE. Following the first observations of eddy coalescence and vertical alignment in the ocean in the 1970s (Cresswell 1982, 1983; Cresswell and Legeckis 1986; Nilsson and Cresswell 1980), vertical alignment of vortices with different densities was studied with analytical and numerical models and in laboratory experiments (Polvani 1991; Nof and Dewar 1994; Carton 2001; Sokolovskiy and Verron 2014). Somewhat surprisingly, no further direct observations of eddy coalescence have ever been reported, albeit numerous observations are suggestive of vertical alignment at work in the ocean. For example, in the Labrador Sea, Lilly et al. (2003) observed several double-core eddies and concluded that vertical alignment of convective lenses of different densities formed during different years is the only plausible generation mechanism of the double-core eddies. In the northwest Pacific Subarctic, Itoh and Yasuda (2010) and Itoh et al. (2011) reported numerous double-core eddies and explained their formation by vertical alignment of lenses with different densities originated in the Kuroshio and Okhotsk Sea. In the northeast Atlantic, the intrathermocline eddy surveyed by Barceló-Llull et al. (2017) in the Canary Basin contained two stacked cores, likely a result of vertical alignment.

Alternative physical mechanisms proposed to explain vertically stacked double thermostads include (i) successive winter cooling events that resulted in capping of an old thermostad with a new thermostad (McCartney and Woodgate-Jones 1991; Brenner 1993); (ii) sinking of thermostads in warm-core rings due to winter cooling (Chapman and Nof 1988); (iii) bottom erosion of thermostad (Brenner et al. 1991; Brenner 1993;

Krom et al. 1992, 1993); (iv) isopycnal injection of a subsurface lens into a larger eddy (Baird and Ridgway (2012)); (v) surface flooding/overwashing/overriding of a subsurface lens with a jet current and trapping of the lens by the meander (Tomosada 1978; Baird et al. 2011; Macdonald et al. 2013). Some of these mechanisms might be at work in the Slope Sea, a wedge-shaped ocean region between the Gulf Stream and North America's eastern seaboard (Csanady and Hamilton 1988). Still, none of the above mechanisms provides a plausible alternative to vertical alignment that explains our observations of a DTE in May 2016. Since Kostianoy and Belkin (1989) reviewed a few instances of DTEs, more observations of DTEs have been made worldwide yet no DTE has ever been described in the Slope Sea. This paper is thus the first account of a DTE in the Slope Sea and at the same time the first report of a double-thermostad WCR of the Gulf Stream.

## 3. Data

### a. Satellite SST imagery

High-resolution (1 km) SST maps from Advanced Very High-Resolution Radiometers (AVHRRs) flown on NOAA polar-orbiting satellites were downloaded from the Rutgers University Coastal Ocean Observation Laboratory's website ([https://marine.rutgers.edu/cool/sat\\_data](https://marine.rutgers.edu/cool/sat_data)) and from the Johns Hopkins University Applied Physics Laboratory Ocean Remote Sensing's website (<http://fermi.jhuapl.edu/>).

### b. Satellite SSH data

Sea surface height (SSH) data are a combination of CNES-CLS13 mean dynamic topography and Ssalto/Duacs daily mean sea level anomaly (with a consistent 1993–2012 reference period). Both are mapped to  $1/4^\circ$  horizontal resolution. CLS Space Oceanography Division produced the mean dynamic topography; Copernicus Marine and Environment Monitoring Service produced and distributed the daily mean sea level anomaly data. Both are available online through AVISO (<http://www.aviso.altimetry.fr>). In this paper we used the SSH data.

### c. CTD

The Sea-Bird Electronics SBE-9/11 Plus CTD probe was cast to sample vertical  $T$ - $S$  structure inside and outside the ring. The CTD data were processed with Sea-Bird Electronics' software. Given the time constraints of the cruise, only two casts were made: one in the ring's center and one just outside the WCR.

### d. XBT

We were fortunate to have several cases of Lockheed Martin Sippican Deep Blue expendable bathythermographs

(XBTs) with a maximum depth of 900 m. These were used to map out the ring's thermal structure along four sections.

#### e. ADCP

The R/V *Endeavor* is equipped with two Teledyne RDI vessel-mounted Ocean Surveyor ADCPs, 75 and 300 kHz, the latter used only in shallow (<100 m) water. The ADCP single ping data (75 kHz) and ancillary sensor data (e.g., GPS and gyrocompass data) were acquired and processed with the University of Hawaii Data Acquisition System (UHDAS). The single ping data were edited by UHDAS prior to averaging into 5-min ensembles. The bin length is 16 m.

#### f. Surface drifters

Three Lagrangian drifters were used to track the movement of surface waters at the center of the ring. Two of the drifters are of the reduced cost design developed by Scott D. Rutherford and collaborators (Leavitt et al. 2015). These were made of four burlap sails measuring 60 cm × 44 cm each attached to a PVC frame containing four sail arms arranged at 90° angles from each other. Each sail is attached to an extension pole (also of 0.5-in. PVC conduit) connecting the deeper sail to a surface plate upon which a WorkWave GPS satellite track pad is mounted. These two drifters had the sails set at 3- and 6-m depth. The third, near-surface drifter was of a similar design by J. Manning and collaborators (Manning et al. 2009). This design similarly utilizes four sails made of vinyl cloth attached to orthogonal fiberglass rods. A 2-in.-diameter, 1.3-m-long PVC cylinder attaches the sails to a surface GPS track pad. Drifter locations at hourly intervals were supplied by J. Manning.

### 4. In situ and satellite observations in May 2016

The Gulf Stream WCR described in this paper was first spotted in satellite SST imagery of 11 May 2016, showing the ring centered at 39°45'N, 66°50'W and impinging on the southern flank of Georges Bank (Fig. 1). Since our cruise target area on Georges Bank (near 41°N, 67°15'W) was located just a few hours of R/V *Endeavor*'s steaming time from the ring's edge, we decided to divert from our cruise plan for 24 h to probe the ring. The fine weather over the Slope Sea immediately prior to the EN578 cruise allowed a few good SST images (Fig. 2) to be acquired and used to estimate direction (azimuth 230°) and speed (7 km day<sup>-1</sup>) of the ring movement and forecast the ring's center location on 22 May (39°20'N, 67°28'W) by linear extrapolation of the ring movement. Based on this forecast, which has turned out to be accurate, we set up a meridional XBT/ADCP line that would cut across the

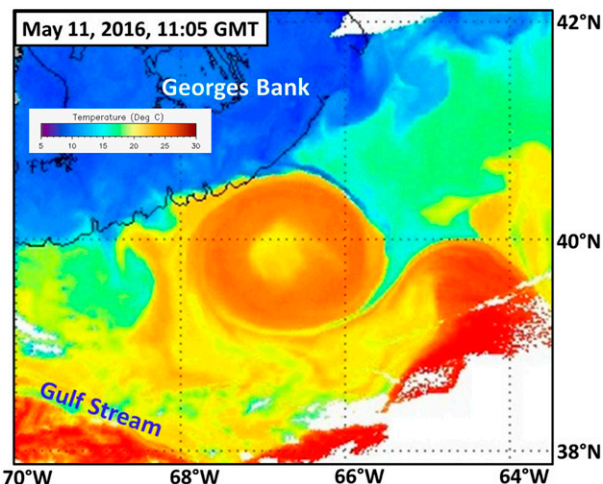


FIG. 1. Satellite SST image acquired at 1105 UTC 11 May 2016, 10 days before our survey. The image shows the warm ring surveyed during the R/V *Endeavor* cruise EN578. The 18°C core of the ring consists of the Sargasso Sea Water. Note the cold streamer being pulled from shelf and the warm streamer in the south coming from the Gulf Stream. The shelf break is approximated by the 180-m isobath, while the shallowest areas of Georges Bank are delineated by the 30-m isobath.

ring center, then added three more XBT/ADCP lines to complete a 3D survey of the ring's thermal structure and velocity field. Two CTD casts, one at the ring center and one just outside, complemented the XBT/ADCP survey. ADCP data were used in real time to optimize the XBT/CTD survey. Three near-surface drifters were launched into the ring center to obtain a Lagrangian view of how well the Sargasso Sea Waters were trapped there.

Underway ADCP 75-kHz data during the rapid XBT/CTD/ADCP survey of the ring on 21–22 May revealed a very well-defined anticyclonic rotation at 50-m depth (Fig. 3). The ring core rotated as a solid body with orbital velocity increasing approximately linearly with distance from the ring center to ~15 km, beyond which it first leveled off for roughly 10 km, then further increased, approaching 1.5 ms<sup>-1</sup> at a radial distance of ~50 km, and then decreased rapidly.

The first and longest XBT section passed within ~10 km of the center, whose location was determined from ADCP data later (see text below). It revealed a peculiar stratification featuring *two* thermostads (Fig. 4). The upper thermostad was located between 100 and 200 m, and the lower one between 250 and 500 m. Both thermostads were well defined with vertically uniform temperatures near the ring center (Fig. 5, top). A CTD cast near the ring center (Fig. 5, bottom) gives us the key properties of both thermostads. The north–south section and radial section to the northwest both came within 10 km of the ring center. The latter 90-km-long

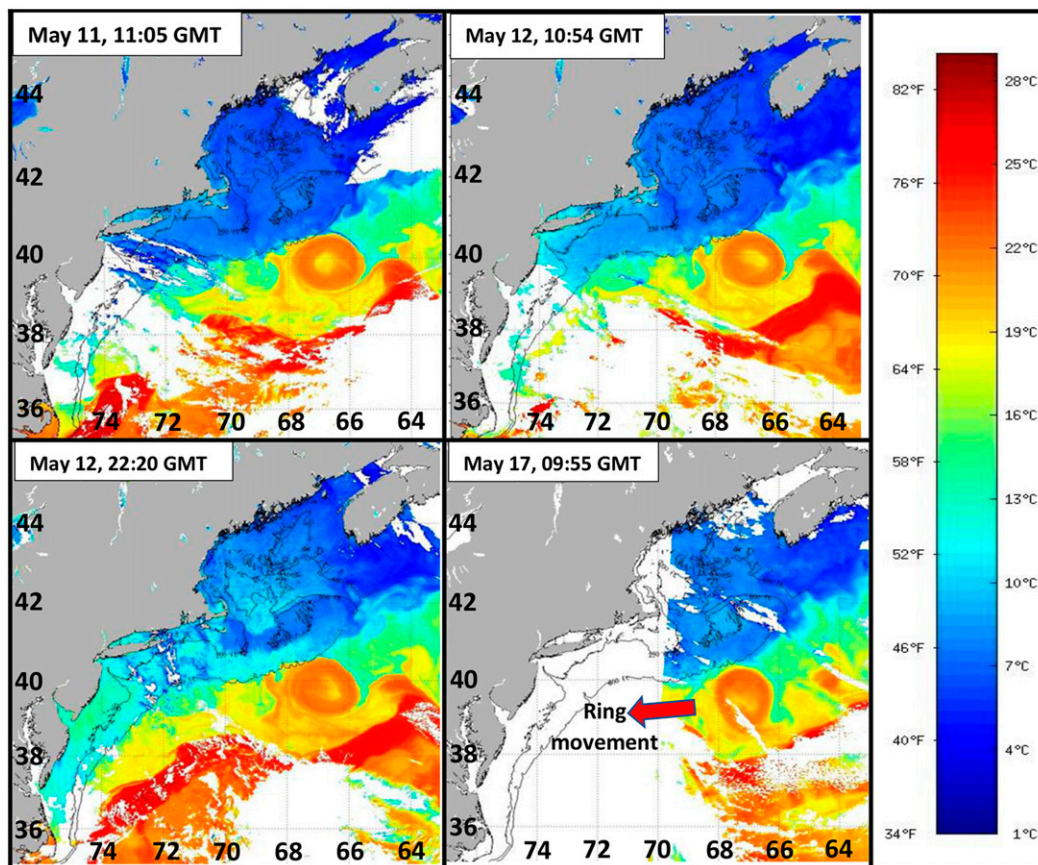


FIG. 2. Satellite SST images from 11 to 17 May 2016, immediately prior to the EN578 cruise. These images were used to estimate direction and speed of the ring movement and set up an XBT line targeting the ring center.

section is bracketed by a CTD at the center and at the end of the radial run along which eight XBTs were taken. The left panel in Fig. 6 shows swirl velocity (normal to the radial section) from ADCP over temperature from XBTs. Near the surface the strongest swirl velocities are located close to 55-km radius, whereas at the lower thermostad maximum speeds lie closer to 40-km radius. The swirl transport can be estimated directly from the velocity field, or geostrophically from the Fofonoff potential energy difference (Fofonoff 1962). The integrals are shown in the right panel of Fig. 6. Using the dashed line in the right panel of Fig. 6 as a measure, an extrapolation of the directly measured velocity integral to 1500 m suggests a total swirl transport of about 36 Sv ( $1 \text{ Sv} \equiv 10^6 \text{ m}^3 \text{ s}^{-1}$ ). As expected, the integral of velocity gives a larger transport than the potential energy difference (36 versus 27 Sv, respectively) because the latter (geostrophic) method does not account for part of the Coriolis acceleration being balanced by the cyclostrophic acceleration, thereby reducing the radial dynamic height or pressure difference to only 0.49 dyn m (4900 hPa), the difference in 0–1500-dbar dynamic height between the

two CTDs. This is particularly relevant for eddies and rings with strong relative vorticity as exemplified by our ring (Fig. 7). The two panels show normalized shear vorticity (top) and curvature vorticity (bottom), respectively. “Normalized” means they have been scaled by the local Coriolis parameter  $f = 0.92 \times 10^{-4} \text{ s}^{-1}$ . The shear vorticity is far noisier because of the short distance over which the shear  $\partial v / \partial r$  is estimated. Nonetheless it shows clearly the transition from negative to positive shear near the radius of maximum velocity ( $\sim 55 \text{ km}$  close to the surface and  $\sim 40 \text{ km}$  at 300-m depth). The curvature vorticity  $v/r$  is far smoother because it is based on swirl velocity, but even it becomes noisy at small radii. Both terms show maximum negative values from  $-0.3f$  to  $-0.4f$  in the central part of the ring.

An effective method for estimating the vertical structure of relative vorticity  $\zeta(z)$  at the center is to fit velocity vectors within a certain distance from the center (here  $< 20 \text{ km}$ ) to an assumed radial parabolic streamfunction  $\Psi(r)$  where  $\zeta = \nabla^2 \Psi(r) = \text{constant}$ , the relative vorticity at  $r = 0$ . The solver used here also gives the best estimate of the ring center at each depth. The method

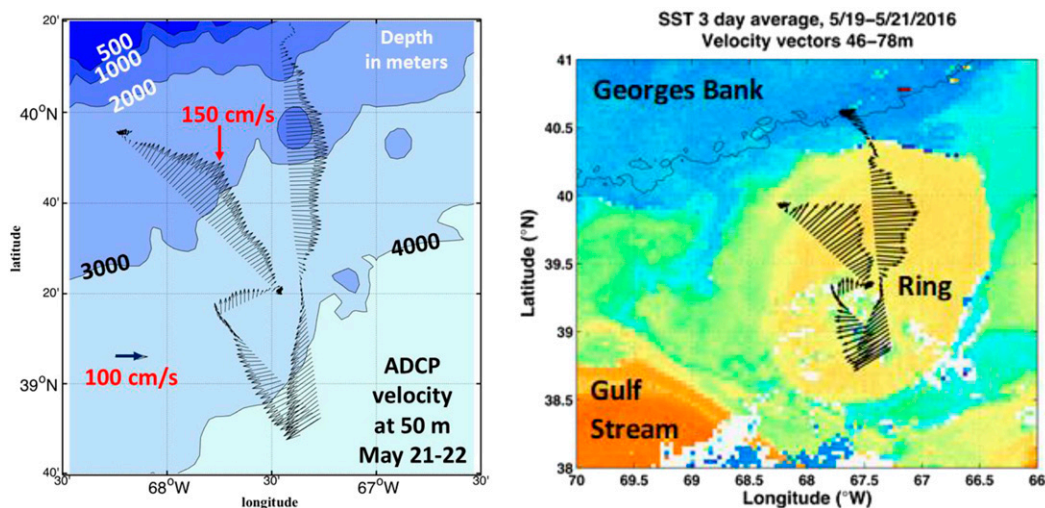


FIG. 3. (left) ADCP 75-kHz horizontal velocity vectors at 50-m depth, 21–22 May 2016 over bathymetry. (right) The same ADCP velocity vectors superimposed over the 3-day composite SST, 19–21 May 2016, downloaded from [http://fermi.jhuapl.edu/avhrr/g\\_s\\_n](http://fermi.jhuapl.edu/avhrr/g_s_n).

used to determine the center vorticity is straightforward (Rossby et al. 2011; Rossby 2014). The basic idea is that the core of the eddy is in solid body rotation. This means that the velocity is circular around the center and increases linearly with distance from the center just like a rotating disc. However, since the center of the eddy is

not perfectly aligned with depth, the center of the velocity field at each depth must be determined as part of the vorticity estimation process. This is done by searching for the position that minimizes the error of the least squares fit of an assumed solid body rotation to the velocity vectors. Thus, the center of the eddy and its

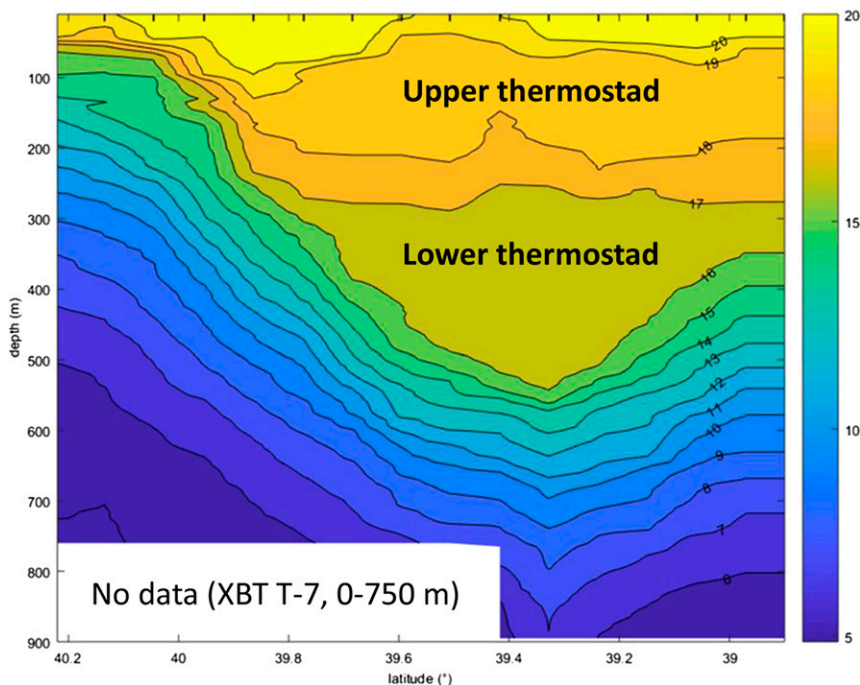


FIG. 4. XBT section along  $\sim 67.4^\circ\text{W}$ , 21–22 May 2016, revealing two vertically uniform layers: the upper  $18^\circ\text{C}$  thermocline at 100–200 m and the lower  $16^\circ\text{C}$  thermocline at 250–500 m. XBT locations are shown with thick ticks at the top. The XBTs (14 in total) were deployed every 10 km. Note deeper XBTs (down to 900 m) south of  $39.42^\circ\text{N}$ .

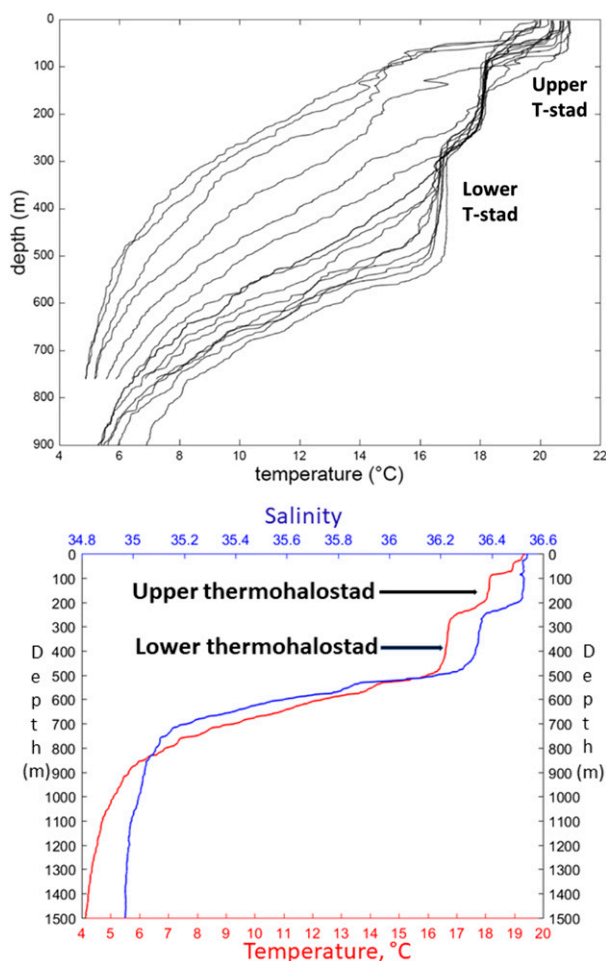


FIG. 5. (top) Vertical XBT profiles of temperature along the 67.4°W section across the ring center, 21 May 2016. Two thermoclines (T-stads) are evident: the upper thermocline between 100 and 200–250 m, and the lower thermocline between 250–300 and 500–550 m. (bottom) Vertical profiles of temperature and salinity in the ring center from CTD cast (1305 UTC 21 May 2016; 39.34°N, 67.48°W), revealing two thermohaloclines: the upper one at 100–200 m (core  $T = 18.14^{\circ}\text{C}$ ,  $S = 36.52$ ) and the lower one at 250–500 m (core  $T = 16.70^{\circ}\text{C}$ ,  $S = 36.35$ ).

relative vorticity at each depth are jointly estimated. The top-left panel in Fig. 8 shows velocity vectors at 61-m depth used to calculate the relative vorticity at that depth. The top-right panel in Fig. 8 shows vertical profile of relative vorticity normalized by  $f$ . The relative vorticity exhibits a minimum of  $-0.8$  between  $\sim 300$ - and  $400$ -m depth, a depth range corresponding to the lower thermocline. The relative vorticity of the upper thermocline between 100 and 200 m is slightly weaker at  $-0.6$ . Given that this layer has different water properties and a different history (next section) this should not come as a surprise. The two bottom panels show tilt and mean velocity of the eddy core as a function of depth. The east–west shift of the eddy core

with depth (Fig. 8, bottom-left panel) appears to be mimicked in the velocity field (Fig. 8, bottom-right panel), whereas in the north–south direction the eddy core is more vertically aligned with  $\sim 0.25 \text{ m s}^{-1}$  translation to the north, but the upper and lower cores are moving at somewhat different speeds.

Another important aspect of the ring’s structure is the ring’s tilt, which is apparent in the north–south section (Fig. 4) and in the plot of ring’s center as a function of depth (Fig. 8, bottom left). The latter reveals a small shift of the upper thermocline relative to the lower thermocline in the north–south direction and a much larger shift in the east–west direction. Another feature of interest is the minimum thickness of the upper thermocline at the ring center along the north–south section (Fig. 4). This is extremely unusual, if not unique, among anticyclonic lens-like eddies that are almost always double convex, with *maximum* thickness at their centers (e.g., Kostianoy and Belkin 1989). To the north of the ring center, the upper thermocline thickens substantially before thinning farther north and disappearing at 39.9°N. To the south of the ring center, the upper thermocline thickens only slightly with almost no hint of thinning farther south, where the ring is close to the Gulf Stream and probably interacts with the latter at times. The north–south asymmetry of the upper thermocline is consistent with the ring being widest at the sea surface, so the ring’s contact with the Gulf Stream takes place first in the surface layer along the southern periphery of the ring. Only as the ring and Gulf Stream become closer, do their subsurface layers start to make contact (Hummon and Rossby 1998).

Three near-surface drifters launched into the ring orbited in expanding loops around its center three times before the two shallowest drifters were swept away by the Gulf Stream. The third drifter—the deepest one—stayed in the ring for 14 days before drifting off to the east. All three drifters remained within 2 km of each other for the first 6 days, and the red and green tracks remained within 2 km of each other for 9 days (Fig. 9).

## 5. Origin and life history of the double-thermocline warm-core Ring C

In this section the life history of the ring is reconstructed from two independent remote sensing data sources: infrared radiometry and satellite altimetry. These two analyses corroborate each other in considerable detail.

### a. Ring’s life history from SST imagery

To reconstruct the life history of the ring, we inspected SST images from 1 September 2015 through 30 June

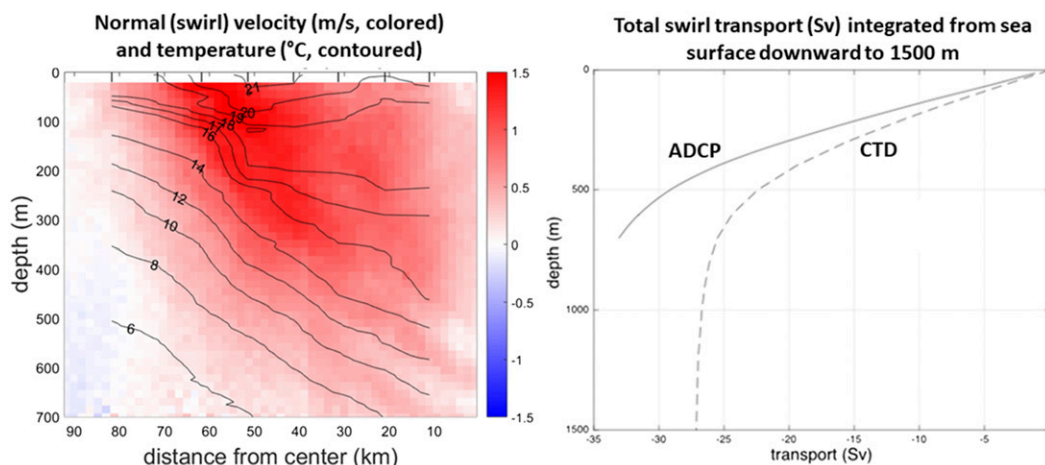


FIG. 6. (left) Vertical section of temperature (contours) and normal (swirl) velocity (colors) along the northwestern radial transect. Short ticks are 10-km marks. Long ticks are XBT locations, 11 km apart. Red and blue colors show flow into and out of the plane, respectively. (right) Total swirl transport (Sv) integrated from the sea surface downward to 1500 m based of the ADCP data (solid line, down to 700 m) and CTD data (dashed line, down to 1500 m) using the Fofonoff potential energy difference. The minus sign means that the flow is anticyclonic.

2016 acquired by AVHRRs on NOAA polar-orbiting satellites. These images are available from the Rutgers University Center of Ocean Observing Leadership (<https://rucool.marine.rutgers.edu/>). During September–October 2015, cloudiness was relatively low; however, the observed pattern of warm-core rings and Gulf Stream meanders differed from that in spring 2016. Little can be said about conditions during winter 2015/16 because of persistent cloudiness that hampered infrared measurements from satellites. Weather conditions steadily improved from late March 2016 onward, allowing a chain of events to be reconstructed. Each developmental stage is documented by at least one satellite image. Most stages are documented by a few images. All images are listed in Table S1 in the online supplemental material. The most important stages are illustrated in Fig. 10. The analysis of SST imagery was compared with and corroborated (and sometimes refined and augmented) by an independent analysis of SSH maps from satellite altimetry (below). Thus, the SST and SSH analyses are mutually consistent. The below timeline includes the following events: 1) formation of Ring A; 2) formation of Ring B; 3) coalescence of Rings A and B into Ring C; 4) Ring C attachment to and interaction with the Gulf Stream; 5) reabsorbance of Ring C by the Gulf Stream.

### 1) FORMATION OF RING A

Ring A is clearly seen for the first time in SST images on 21 February, centered at 41.3°N, 63.5°W, with a diameter of 120 km (Fig. 10). The persistent cloudiness during the preceding two months precludes any definitive conclusion about its formation to be derived from

SST imagery alone. Fortunately, SSH maps fill the gap in SST imagery and reveal that Ring A was born from a Gulf Stream meander, which on 25 December 2015 can be seen centered at 40.5°N, 62°W, almost pinched off and detached from the Gulf Stream (see supplemental material). This analysis implies a slow movement of Ring A toward west-northwest over the two intervening months (between 25 December 2015 and 21 February 2016) with the average speed of <3 km per day, which is within the observed range of westward propagation

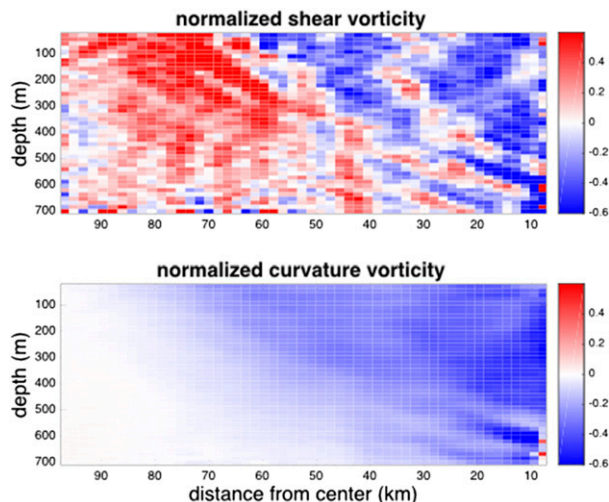


FIG. 7. Vertical sections of (top) shear vorticity  $\partial v/\partial r$  and (bottom) curvature vorticity  $v/r$  along the northwestern radial transect. Blue (red) means negative (positive) shear. The values have been scaled by the local Coriolis parameter. The velocity field has been smoothed radially for scales  $< \sim 7$  km.

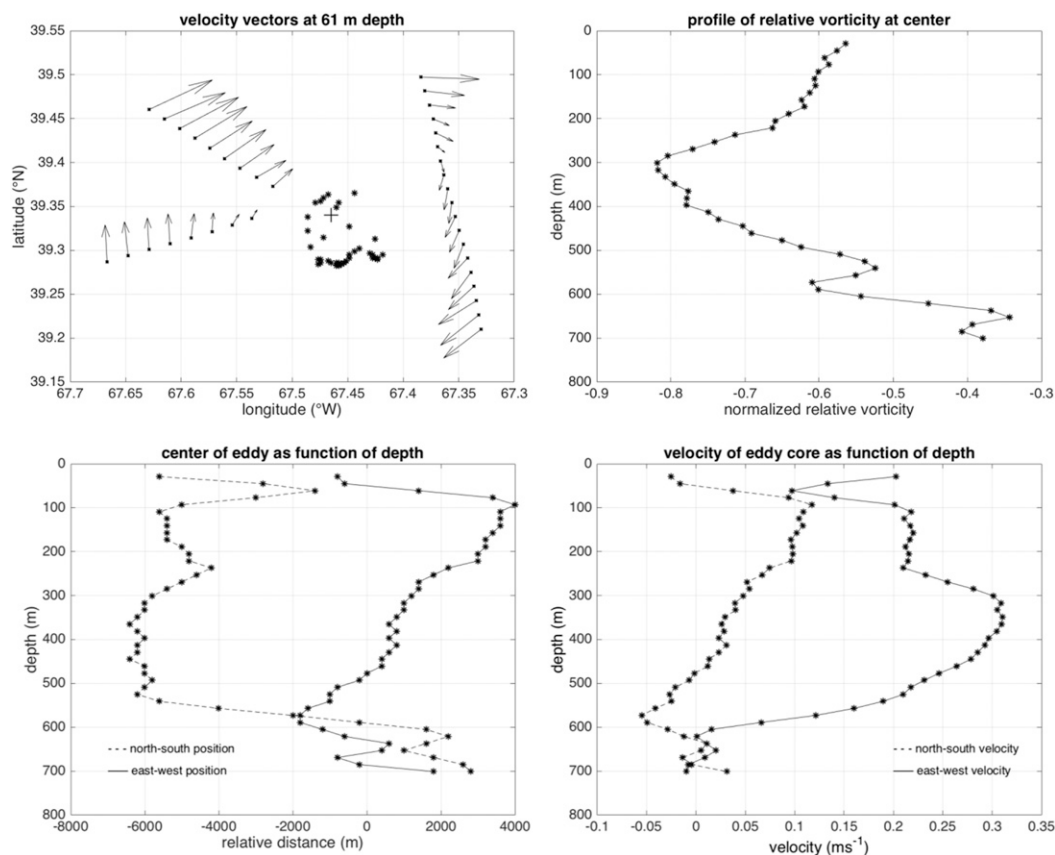


FIG. 8. (top left) Velocity vectors at 61-m depth within 20 km of the center CTD (+); asterisks (\*) show the scatter in the ring's estimated center from the least squares fit estimation of relative vorticity  $\zeta$  for each depth. (top right) Vertical structure of relative vorticity  $\zeta$ . (bottom left) Estimated center of the ring as a function of depth. (bottom right) Velocity of the ring's core (as a simple average of all vectors) as a function of depth.

speed of warm-core rings of the Gulf Stream in the Slope Sea (Olson 1991). Ring A continued its migration toward west-southwest, reaching 40.8°N, 65°W on 16 March.

## 2) FORMATION OF RING B

Ring B was born on 16–17 March from a large meander of the Gulf Stream at 40.5°N, 61.5°W (Fig. 11). A week later, on 24–25 March, the newly born Ring B is seen in SST, centered at 40.4°N, 62.9°W, while Ring A is centered at 40.8°N, 65.3°W (Fig. 10). Ring B is slightly elliptical, with the long axis of 200 km, while Ring A is roughly circular, with a diameter of 120–150 km. The rings are just 55 km apart, with a cold streamer of Georges Bank Water in between. Ring B migrates westward and begins interacting with Ring A by 28 March.

## 3) COALESCENCE OF RINGS A AND B INTO RING C

The 4 April SST map (see supplemental material) shows a large segment of a warm ring centered near 40°N, 64°W and mostly obscured by clouds. This is

likely Ring B that moved westward along 40°N from 63°W on 25 March to 64°W by 11 April, covering 85 km in 17 days with a speed of 5 km day<sup>-1</sup>. The 11 April SST map (Fig. 10) shows Rings A and B merged into a single Ring C centered at 40°N, 65°W. From SSH maps (Fig. 11), Rings A and B began coalescing around 29 March and merged into a single Ring C by 6 April.

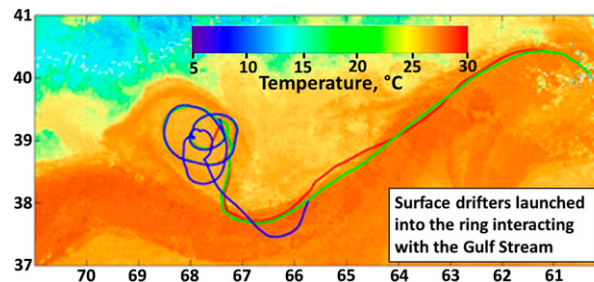


FIG. 9. The 16-day tracks of three drifters launched into the ring, from 21 May to 6 June 2016. Drogue depths: red, 1 m; green, 3 m; blue, 6 m. Background: composite SST map for 24–30 May 2016 downloaded from [http://fermi.jhuapl.edu/avhrr/g\\_s\\_n](http://fermi.jhuapl.edu/avhrr/g_s_n).



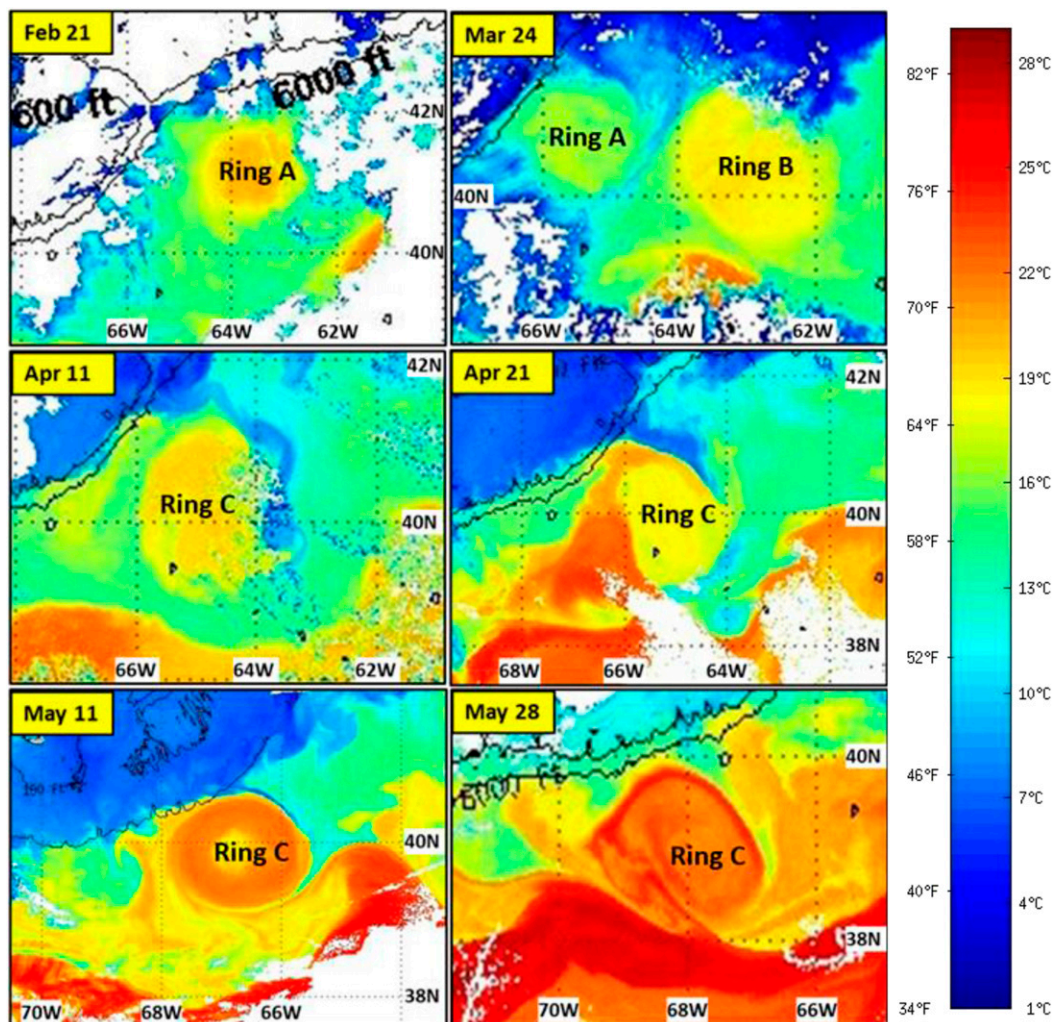


FIG. 10. Selected SST images showing Ring A (21 Feb) and Ring B (24 Mar), their merger and formation of Ring C (11 Apr), its interaction with the Gulf Stream (21 Apr), detachment from the Gulf Stream (11 May), and reapproach to the Gulf Stream (28 May) shortly before its eventual reabsorbance by the Gulf Stream by 1 Jun.

It is conjectured that the Ring C's double-thermostad stratification (Figs. 4 and 5) resulted from vertical alignment of rings A and B. During this process, the younger, warmer, and lighter Ring B overrode the older, colder, and denser Ring A. Ring B formed the upper thermostad, while Ring A formed the lower thermostad, of Ring C.

#### 4) AXISYMMETRIZATION OF RING C, ENTRAINMENT OF STREAMERS, AND REATTACHMENT TO THE GULF STREAM

Once formed, Ring C had an elongated shape, an evidence of incomplete vertical alignment of Rings A and B. Axisymmetrization of Ring C took place between 8 April and 9 May. In the 11 May SST image, Ring C is nearly circular (Fig. 1). Later, Ring C appears to be

increasingly elliptic (Fig. 10) until it starts reattaching to the Gulf Stream around 25 May. In April–May, Ring C interacted with the Gulf Stream by pulling a warm streamer, while also pulling a cold streamer from Georges Bank. Eventually, the warm streamer prevailed over the cold streamer and completely encircled Ring C (Fig. 10). The vertical and horizontal structure of Ring C could have in part resulted from the ring interaction with the Gulf Stream.

#### 5) REABSORBANCE OF RING C BY THE GULF STREAM

On 25 May, Ring C, still separate and distinct, is connected to the Gulf Stream with a warm streamer (see supplemental material). By 28 May, Ring C is dominating a large, strongly asymmetric mushroom-like dipole

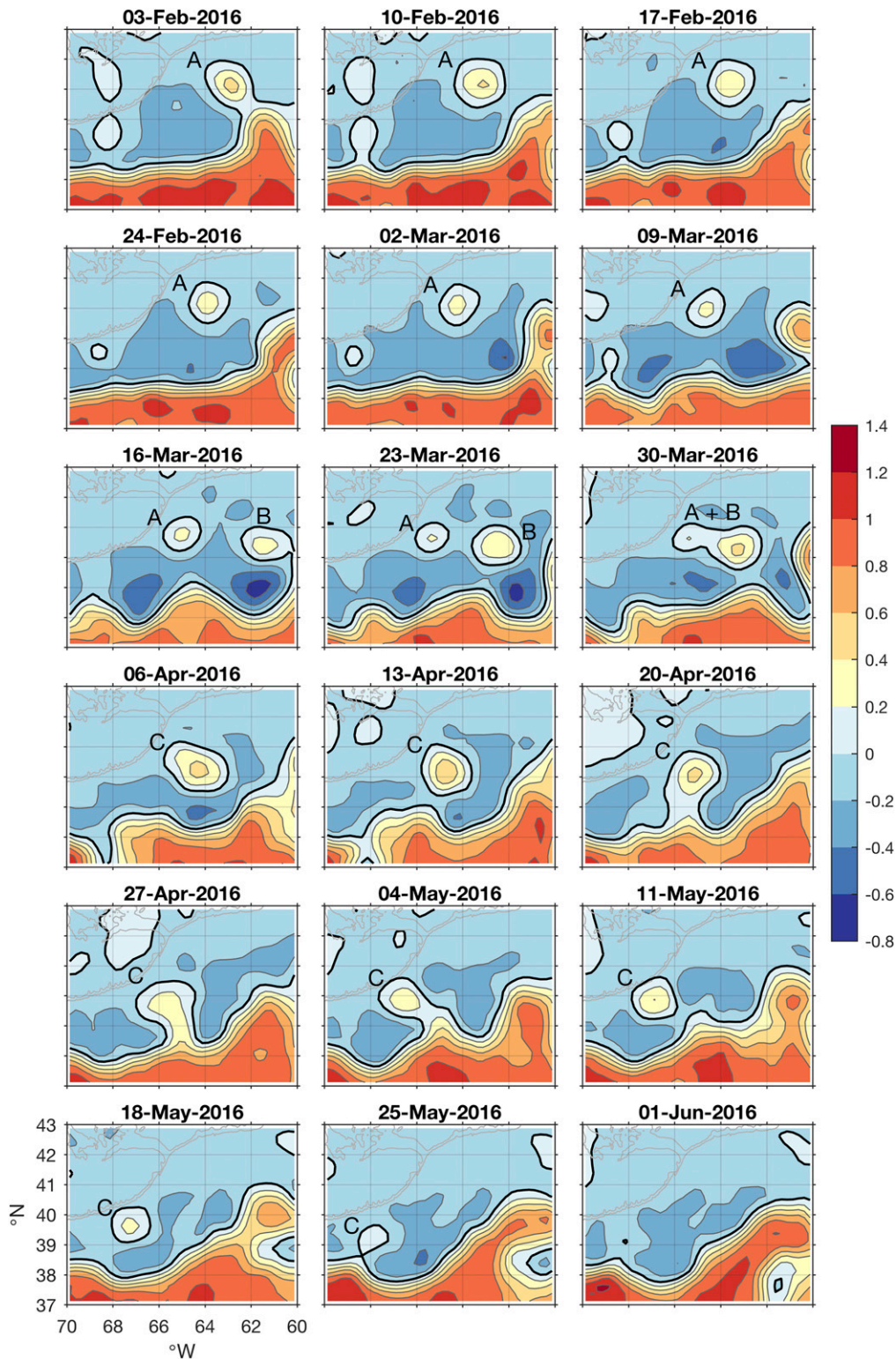


FIG. 11. Weekly SSH maps showing the formation of Ring A (10 Feb) and Ring B (16 Mar), their merger (A + B; 30 Mar) and formation of Ring C (6 Apr), its interaction with the Gulf Stream (20 Apr–4 May), detachment from the Gulf Stream (11 May), and eventual reabsorbance by the Gulf Stream (1 Jun). Contour interval is 20 cm. The thick black line is the 0-cm contour. The two thin light gray lines are 200- and 1000-m isobaths. The color scale on the right shows SSH in meters.

(150 km  $\times$  200 km) that formed rapidly between 25 May and 28 May. During that time, the previously nearly circular Ring C morphed into a spiral eddy vigorously interacting with the Gulf Stream (Fig. 10). Eventually, the Gulf Stream absorbed Ring C by 1 June (Fig. 11).

*b. Ring's life history from satellite altimetry SSH maps*

Daily SSH maps covering the 37°–43°N, 70°–50°W area for one year (1 July 2015–30 June 2016; see supplemental material) were analyzed to reconstruct the life of Ring C. The most important period in February–May 2016 is illustrated by weekly SSH maps for the 37°–43°N, 70°–60°W area (Fig. 11). During the year-long time span of our analysis, numerous WCRs were spawned by anticyclonic meanders of the Gulf Stream. These WCRs traveled west and eventually got absorbed by the Gulf Stream. Given the relatively short time between ring formation and its absorbance by the Gulf Stream, most rings had no chance to interact with other rings. Not surprisingly, just two events of ring-to-ring interaction were observed, of which only one event described in this paper led to coalescence of two rings. The life of Ring C is traced back to 25 December 2015 when a warm-core ring (Ring A) formed near 40.5°N, 62°W. Immediately after formation, the ring migrated westward to 63°W before returning to the Gulf Stream, approaching, attaching, and interacting with the Gulf Stream from 5 January through 6 February 2016. On 6 February, Ring A pinched off the Gulf Stream at 41°N, 63°W with a maximum SSH anomaly  $> 40$  cm relative to surrounding waters (Fig. 11). The ring migrated west-southwest while decreasing in amplitude, reaching 40.8°N, 65°W on 16 March. By this time, another large meander has formed to the east and another warm-core ring (Ring B) pinched off the Gulf Stream on 16–17 March at 40.5°N, 61.5°W. Ring B migrated westward and began interacting with Ring A by 28 March. Between 29 March and 5 April, Ring A and Ring B coalesced into Ring C. By 12 April, Ring C became more circular before it started interacting with the Gulf Stream between 14 April and 9 May. On 10 May, Ring C detached from the Gulf Stream near 39.75°N, 67°W and headed southwest reaching 39.5°N, 67.5°W by 22 May. By this time, its amplitude decreased from about 40 cm on 10 May to under 20 cm on 25 May, when Ring C approached and reattached to the Gulf Stream and was finally reabsorbed by the Gulf Stream around 1 June.

*c. Comparison of life histories of Ring C from SST and SSH*

The life histories of Ring C derived from SSH and SST are entirely consistent except, seemingly, for the very end of the ring's life in late May when Ring C remained

near the Gulf Stream before it was finally reabsorbed by the Gulf Stream around 1 June. During that time, the ring's amplitude in SSH decreased to  $< 20$  cm on 25 May. The ring's signal in SSH maps is probably underestimated. Indeed, during our survey on 21–22 May, the dynamic height difference between the center and the outside of the ring was 45 cm, more than twice the ring's amplitude in SSH on 25 May. The only alternative—and highly unlikely—explanation of the much smaller SSH signature of the ring is an extremely rapid loss of the ring's signal in SSH from 45 cm on 21–22 May (according to our ship survey) to  $< 20$  cm on 25 May (according to SSH maps). The underestimation of the ring's strength in SSH maps is not surprising since SSH is a smoothed field that does not retain the full amplitude of SSH variations at scales  $< 50$  km (Stammer and Theiss 2004), which is the scale of Ring C defined as the radial distance from its center to the maximum velocity locus (55 and 40 km for the upper and lower thermostad, respectively). The most important formation stages of the double-thermostad Ring C based on SST and SSH data as well as our XBT/CTD survey are shown in Fig. 12.

## 6. Discussion

*a. Formation of Ring C due to vertical alignment of Rings A and B*

The diverse set of in situ and satellite data presented in previous sections is interpreted as coalescence and vertical alignment of two rings (A and B) that form a double-thermostad ring (C), with Ring A becoming the lower thermostad and Ring B becoming the upper thermostad, of Ring C. Kinematical aspects of this process inferred independently from SST and SSH data are clear: once formed, Ring B moved westward much faster than Ring A, eventually interacting with and apparently overriding Ring A (Figs. 10 and 11). This interpretation (coalescence of Rings A and B) is the only plausible scenario that explains the sudden disappearance of Ring A from satellite imagery (both SST and SSH). Our XBT/CTD data (Figs. 4 and 5) support this scenario since the upper and lower thermostads of Ring C have temperatures similar to SSTs observed in, respectively, rings B and A before their merger. The upper thermostad in Ring C had the vertically averaged temperature of 18.1°C in its center, while Ring B had SST of 18°–19°C in its center before the coalescence of Rings A and B; the lower thermostad in Ring C had the vertically averaged temperature of 16.7°C in its center, while Ring A had SST of 16°–17°C in its center before the coalescence of Rings A and B.

The 1.4°C temperature difference between the upper thermostad (18.1°C) and lower thermostad (16.7°C) in

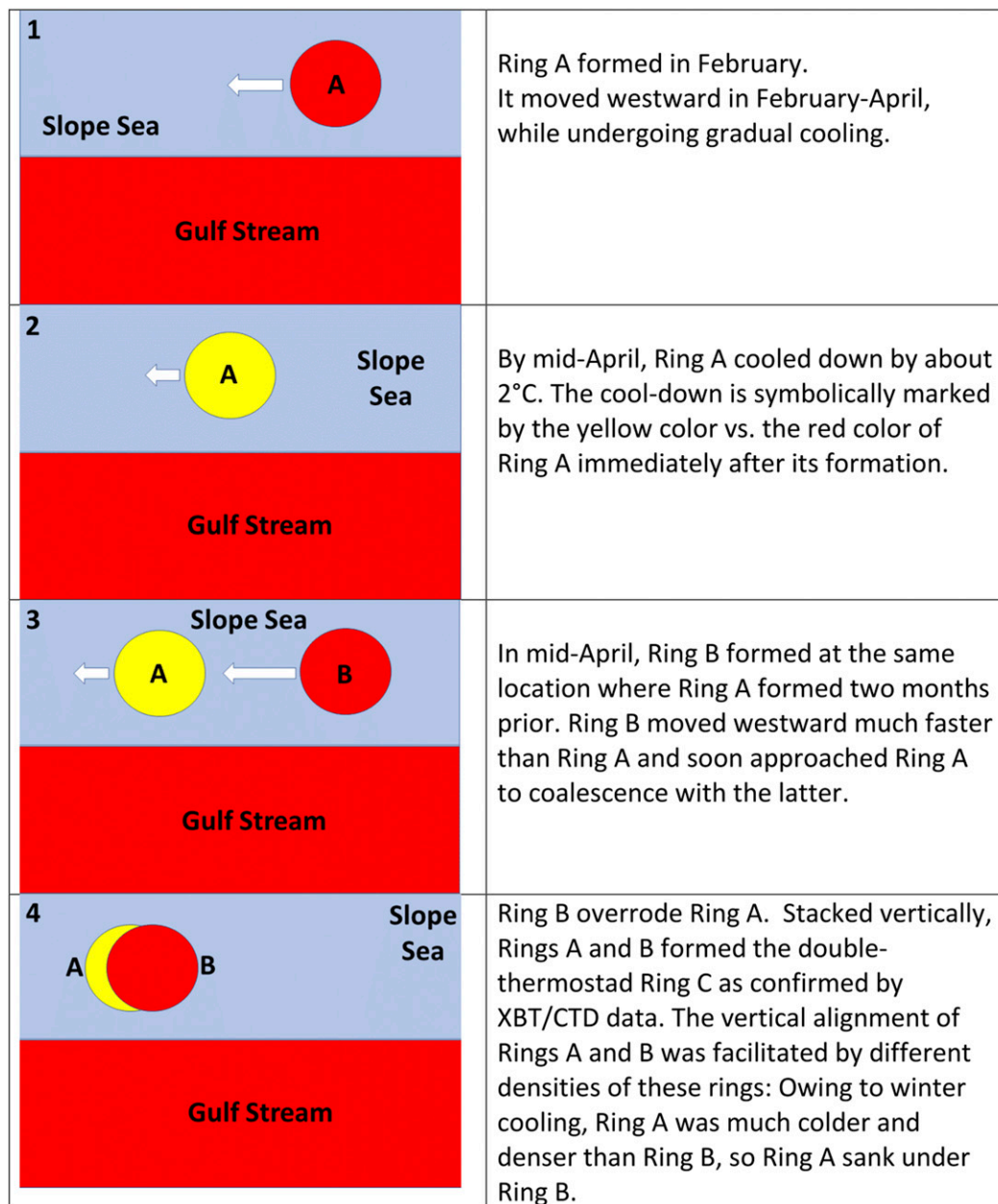


FIG. 12. Main formation stages of Ring C illustrated by four highly simplified plane view schematics. North is on top. Rings are shown circular and of the same size while actual Rings A and B are of different sizes and elliptical at times. The last plate (stage 4) shows Rings A and B shortly before Ring B overrides Ring A and vertical alignment of these rings creates the double-thermostat Ring C surveyed in our cruise. During stage 3, Ring A was hardly moving westward; if anything, Ring A moved slightly eastward, toward Ring B, consistent with vortex-to-vortex interaction during vertical alignment.

Ring C is explained by cooling of Ring A between its formation in February and its coalescence with Ring B in April. Indeed, the 1.4°C cooling over two months implies a moderate cooling rate of about 0.7°C month<sup>-1</sup>, consistent with numerous observations and modeling studies of warm-core Gulf Stream rings in the same

region (Schmitt and Olson 1985; Dewar 1986; Olson 1991). Even faster cooling rates have been reported in the Slope Sea, for example, the warm-core ring 82-B cooled by 2°C, from 17.7° to 15.7°C, in just one month between mid-March and mid-April 1982 (Schmitt and Olson 1985).

*b. How rare are double-thermostad WCRs of the Gulf Stream?*

The absence of previous reports of double-thermostad WCRs of the Gulf Stream might appear surprising, especially given the abundance of in situ observations and frequent formation of WCRs, in the Slope Sea. According to a 5-yr (1980–85) climatology of the Gulf Stream and its rings (Auer 1987), 22 WCRs are formed and absorbed by the Gulf Stream annually between 44° and 75°W, with the maximum frequency of WCR formation near the New England Seamounts. In 11 cases (all between 55.1° and 67.5°W), a WCR was absorbed by another WCR, averaging two WCR mergers a year. Some mergers could produce double-thermostad WCRs provided enough density difference between two coalescing WCRs. Lacking such a differential, no vertical alignment would occur, hence no DTE formation.

The most recent census of WCRs (Monim 2017) netted 536 WCRs in 17 years (2000–16) between 75° and 55°W, averaging roughly 32 WCRs per year in an area 50% smaller than in Auer (1987). Even though the WCR annual formation rate (per 1° of longitude) in Monim (2017) is about twice that in Auer (1987), absorbance of one WCR by another is exceedingly rare, normally one or two events per year.

Our analysis of satellite altimeter SSH maps confirms the above estimates based on the Auer (1987) results. A careful inspection of the year-long SSH animation based on daily SSH maps from August 2015 to July 2016 (see supplemental material) revealed just two cases of a WCR merger, including one incomplete merger before both WCRs were reabsorbed by the Gulf Stream. The only complete merger occurred in April 2016, with R/V *Endeavor* having documented the merger's product (double-thermostad Ring C) with in situ data, augmented by satellite data, both reported in this paper.

*c. Double-thermostad eddies in the World Ocean*

1) FORMATION MECHANISMS OF  
DOUBLE-THERMOSTAD EDDIES

*(i) Vertical alignment*

Following the first observations of eddy coalescence in the ocean (Cresswell 1982, 1983; see also Cresswell and Legeckis 1986; Nilsson and Cresswell 1980), vertical alignment of vortices with different densities (Polvani 1991) was studied analytically and in laboratory experiments (e.g., Nof and Dewar 1994). Numerous theoretical and experimental studies followed, reviewed recently by Sokolovskiy and Verron (2014). Somewhat surprisingly, no further direct observations of eddy coalescence have ever been reported. Yet numerous

observations are suggestive of vertical alignment at work in the ocean. For example, in the Labrador Sea, Lilly et al. (2003) observed several double-core eddies and concluded that vertical alignment of convective lenses of different densities formed during different years is the only plausible generation mechanism of the double-core eddies. In the northwest Pacific Subarctic, Itoh and Yasuda (2010) and Itoh et al. (2011) reported numerous double-core eddies and explained their formation by vertical alignment of lenses with different densities that originated in the Kuroshio and Okhotsk Sea. In the northeast Atlantic, the intrathermocline eddy surveyed by Barceló-Llull et al. (2017) in the Canary Basin contained two stacked cores, likely a result of vertical alignment.

*(ii) Successive winter cooling events*

Schmitt and Olson (1985) modeled evolution of a warm-core ring due to winter convection. Dewar (1986) modeled evolution of winter mixed layer in warm-core rings. McCartney and Woodgate-Jones (1991) observed a double-thermostad eddy in the South Atlantic and suggested that the double thermostad was generated by successive winter cooling events that resulted in capping of an old thermostad with a new thermostad. Successive winter cooling events were suggested by Brenner (1993) to explain the double thermostad in the Cyprus Eddy (Brenner 1993).

*(iii) Sinking of thermostads*

Chapman and Nof (1988) proposed sinking of thermostads in warm-core rings due to winter cooling.

*(iv) Bottom erosion of thermostad*

Brenner et al. (1991), Brenner (1993), and Krom et al. (1992, 1993) presented observations of long-term evolution of the Cyprus Eddy that provided direct evidence of bottom erosion of the eddy's deep thermostad (down to 450 m). Following the bottom erosion of the 450-m thermostad, a lower secondary thermostad was formed, extending to 650 m. These observations are unique since not only the secondary thermostad is substantially (by 1°C) colder than the upper thermostad but it is also 200 m deeper than the original 450-m thermostad.

*(v) Isopycnal injection of a subsurface lens into a larger eddy*

In the Tasman Sea, Baird and Ridgway (2012) observed anticyclonic eddies containing lenses of Bass Strait Water that have likely been injected into the eddies by advection along isopycnals. The same mechanism may be at work in other regions where alien waters are isopycnally injected at intermediate depths.

TABLE 1. Double thermostads in Gulf Stream warm-core rings in the Slope Sea.

Ring	Dates	Ship, cruise	Thermostads	Reference
77-G	31 Aug 1977	<i>Tamaroa</i> 77-08	18°, 12°C	Cook (1979)
77-G	17 Aug 1977	<i>Endeavor</i> -11	18°, 12°C	Richardson (1980)
79-H	1 Jul 1980	<i>Mormac Argo</i> 80-08	16°, 12°C	Hughes and Cook (1983)
79-K	16 May 1980	<i>George B. Kelez</i> 80-02	Deep 13°C	Hughes and Cook (1983)
81-F	28 Nov 1981–17 May 1982	<i>Oleander</i> 82-04, 82-05, 82-06	Deep 12°–13°C thermostad	Fitzgerald and Chamberlin (1984); Cerone (1984, Fig. C-52); Cook (1985)
EN578	May 2016	<i>Endeavor</i> EN578	18.1°, 16.7°C	This paper

Foremost candidates are (i) the Indian Ocean where lenses of Red Sea Water could penetrate warm eddies of the Somali Current, and (ii) eastern North Atlantic, where lenses of Mediterranean Water could penetrate large mesoscale eddies west of Gibraltar.

(vi) *Surface flooding/overwashing/overriding of a subsurface lens with a jet current and trapping of the lens by the meander*

Tomosada (1978) presented detailed observations of a large warm eddy overridden by the Kuroshio. A similar process was observed in the Tasman Sea where anticyclonic eddies were subject to surface flooding by the East Australian Current (Baird et al. 2011; Macdonald et al. 2013). There is little doubt that surface flooding/overwashing/overriding of warm-core rings by anticyclonic Gulf Stream meanders occurs in the Slope Sea, although observations of this phenomenon are absent.

## 2) OBSERVATIONS OF DOUBLE-THERMOSTAD EDDIES IN THE WORLD OCEAN

The first observations of double-thermostad eddies were made in the 1970s. Such peculiar eddies were likely observed before, yet those observations were overlooked, misinterpreted, or eliminated (redacted) during quality checks and data processing, particularly while contouring vertical sections from sparse data. For example, the discovery of intrathermocline eddies in the Arctic Ocean did not happen until early 1970s, although such eddy currents were first observed in 1937 but were completely misinterpreted (see Kostianoy and Belkin 1989, and references therein). Another example is from Hallock et al. (1981, p. 1675): “During the survey, shipboard data processing revealed a very peculiar CTD profile at Station 18. . . . A layer of homogeneous water was observed between 690 and 840 m depth. An instrument malfunction was immediately suspected and it was not until the same feature had been detected in data from adjacent XBT profiles that the CTD profile was accepted as valid.”

### (i) Slope Sea

We searched the literature for reports of double-thermostad warm-core rings in the Slope Sea to no avail. Nonetheless, we found a few published XBT sections across Gulf Stream WCRs that reveal such double thermostads, briefly described below and summed up in Table 1:

Ring 77-G was crossed twice in two weeks: first, on 17 August 1977 during the R/V *Endeavor* cruise 11 (Richardson 1980, Fig. 5b) and second, on 31 August 1977 during the USCGC *Tamaroa* cruise 77-08 (Cook 1979, Fig. 10). Both sections revealed two distinct thermostads. Judging from the depth of 12°C isotherm (respectively, 500 versus 350 m), the *Endeavor* section hit the ring center, while the *Tamaroa* section missed it. The ring center featured a relatively thin upper thermostad in the 40–100-m layer with  $T = 18^\circ\text{C}$  and a thick lower thermostad in the 250–500-m layer with  $T = 12^\circ\text{C}$ .

Ring 79-H was crossed on 1 July 1980 during the R/V *Mormac Argo* cruise 80-08 (Hughes and Cook 1983). The ring’s upper thermostad at 50–200 m was relatively cold ( $T = 16^\circ\text{C}$ ), while the lower thermostad at 270–350 m had  $T = 12^\circ\text{C}$ . Schmitt and Olson (1985, p. 8834) noted “a variety of model runs suggests that the coldest water likely to be found in a winter-cooled warm ring is about 12°C under normal climatic conditions in the slope water. We note that isothermal cores of 13.0° and 12.3°C were observed in WCR 81F and in a warm ring sampled by D. Kester (reported by Richardson [1980]).” The warm ring sampled by Dana Kester on the last day of R/V *Endeavor* cruise 11 was later identified as WCR 77-G (Cook 1979). Cerone (1984, p. 57, Table 1) listed ring 77-G as a merger of two “old” rings, 77-D and 77-E. The only other merger listed by Cerone (1984, p. 57, Table 1) is the coalescence of 78-E and 78-F into 78-H.

Ring 81-F mentioned by Schmitt and Olson (1985) was sampled by R/V *Oleander* in cruises 82-04/05/06 between 28 November 1981 and 17 May 1982

TABLE 2. Lower thermostads in double-thermostad eddies in the Sargasso Sea.

Reference	Ship, cruise, station	Date	Lat/lon	Depth (m)	$T$ ( $^{\circ}\text{C}$ )	$S$	Density
Leetmaa 1976	R/V <i>Researcher</i> , XBT 565	30 Apr 1976	28.35 $^{\circ}$ N, 69.42 $^{\circ}$ W	600–760	14–15	—	—
Hallock et al. 1981	USNS <i>Kane</i> , station 18	11 Aug 1979	31 $^{\circ}$ N, 72.5 $^{\circ}$ W	690–840	16	36.3	26.75 Sigma- $t$
Zantopp and Leaman 1982	R/V <i>Columbus Iselin</i> , station I8028	20 Nov 1980	25.48 $^{\circ}$ N, 70.75 $^{\circ}$ W	650–730	15	36.1	26.8 Sigma- $\theta$
Brundage and Dugan 1986	Ship unknown, XBT 199	31 Jul 1981	30 $^{\circ}$ N, 69 $^{\circ}$ W	650–800	15–16	—	—

(Fitzgerald and Chamberlin 1984; Cerone 1984, Fig. C-52; Cook 1985).

Ring 79-K provides another, previously unidentified example of deep convection in a warm ring. Indeed, the XBT section across this ring on 16 May 1980 during the R/V *George B. Kelez* cruise 80-02 revealed a very deep (>400 m) 13 $^{\circ}$ C thermostad (Hughes and Cook 1983).

#### (ii) Sargasso Sea

The first brief report of a double-thermostad eddy by Leetmaa (1976) was followed by Hallock et al. (1981), Zantopp and Leaman (1982), and Brundage and Dugan (1986) who documented double-thermostad eddies featuring a very thick, 500-m deep, 18 $^{\circ}$ C thermostad underlain by a much thinner (100–200 m) 14 $^{\circ}$ –16 $^{\circ}$ C thermostad centered around 700 m (Table 2). The lower thermostads' characteristics in Table 2 are suggestive of their origin in the Slope Sea as cores of overwintered warm rings of the Gulf Stream—the scenario proposed by Schmitt and Olson (1985) for numerous isothermal lenses found in the Gulf Stream recirculation area.

#### (iii) East Australian Current/Tasman Sea

Three mechanisms were observed creating double-thermostad eddies in the Tasman Sea:

Vertical alignment: Cresswell (1982, 1983) and Cresswell and Legeckis (1986) documented two mergers of anticyclonic eddies of the East Australian Current: eddies I and J in 1979–80, and eddies Leo and Maria in 1980. In each case, two eddies aligned vertically according to their densities. In retrospect, Cresswell (1983) concluded that eddy A in 1977 may have been formed by coalescence of two eddies since eddy A had two thermostads as documented by Nilsson and Cresswell (1980, Fig. 8).

Isopycnal injection: A different mechanism generates double-core anticyclonic eddies reported by Baird and Ridgway (2012) in Tasman Sea, where they found several eddies containing lenses of alien water, which turned out to be the Bass Strait Water. In winter,

these lenses cascade down the continental slope east of the Bass Strait and spread isopycnally across the Tasman Sea, where they occasionally penetrate rings spawned by the East Australian Current.

Surface flooding/overwashing: Baird et al. (2011) and Macdonald et al. (2013) reported surface flooding of anticyclonic eddies by meanders of the East Australian Current.

#### (iv) Northwest Pacific Subarctic

The rich frontal structure of this region is conducive to the formation of multilayer eddies, particularly north of the Kuroshio. Tomosada (1978) described a large double-core warm eddy detached from the Kuroshio and pointed out that such warm eddies (rings) often have two cores (isostads), with the lower core (10 $^{\circ}$ –11 $^{\circ}$ C) being a remnant of winter convection (wintered water). Belkin and Mikhailichenko (1986) observed a double-core anticyclonic eddy with the 16 $^{\circ}$ C Subtropical Mode Water in the 150–300-m layer and the 12 $^{\circ}$ C water at 400–500 m. Bogdanov et al. (1985) observed an anticyclonic eddy with two cold thermostads, at 100–400 m with  $T = 8^{\circ}$ –9 $^{\circ}$ C and at 600–800 m with  $T = 5^{\circ}$ C. Rogachev et al. (2007) presented sections across double-core anticyclonic eddies generated by the Alaskan Stream/Aleutian Current. Itoh and Yasuda (2010) reported numerous double-core anticyclonic eddies, with the upper core from the Kuroshio Extension and the lower core from the Okhotsk Sea, and suggested that the double-core structure is created by vertical alignment of eddies with different densities (Polvani 1991). Itoh et al. (2011) continuously observed such a double eddy for over a year. Kaneko et al. (2015) documented evolution of a multi-layer anticyclonic eddy that resembled some double-core eddies observed in the Kuroshio–Oyashio current system.

#### (v) South Atlantic: Agulhas Rings

Vertical temperature profiles in centers of Agulhas warm anticyclonic eddies (rings) and inside the Agulhas Retroflection reveal double thermostads (Gordon et al. 1987, Fig. 14; Olson et al. 1992, Fig. 2). When van Aken

et al. (2003) surveyed a young Agulhas ring Astrid in 2000, they found two layers with local minima of potential vorticity (pycnostads); the lower layer was a lens of the Subantarctic Mode Water isopycnally advected into the ring. McCartney and Woodgate-Jones (1991) discovered a double-thermostad eddy in the South Atlantic. The eddy has turned out to be a warm-core ring spawned by the Agulhas Current Retroflexion. The double-thermostad stratification was explained to be a result of two successive winters' cooling events.

While studying hydrographic fronts in the Southern Ocean, Belkin and Gordon (1996) analyzed vertical sections across the Agulhas Retroflexion. Vertical temperature profiles inside the Retroflexion have shown a 100-m-thick lens (secondary thermostad) located beneath the main thermostad. However, when the same temperature data have been previously contoured by the data originators for a cruise report, the secondary thermostad was eliminated by excessive smoothing applied during the contouring, resulting in evenly spaced isotherms—thus no lens—all the way down to the maximum depth of the vertical section. There is no doubt that numerous lenses elsewhere worldwide have been eliminated in the same fashion during contouring. A careful examination of vertical sections using original observed data is therefore warranted.

#### (vi) Mediterranean Sea: Cyprus Eddy

Brenner et al. (1991), Brenner (1993), and Krom et al. (1992, 1993) documented development of a secondary thermostad in the quasi-stationary anticyclonic warm-core Cyprus Eddy south/southeast of Cyprus. Brenner et al. (1991) observed erosion of the bottom of the Eddy's thermohalostad: "In Fig. 4 we also note the gradual erosion of the lower part of the thermostad presumably due to mixing with water from below." Brenner (1993) suggested that the double thermohalostad could be a result of two successive winters' convective events. Vertical profiles in Krom et al. (1992, Fig. 3) and Krom et al. (1993, Fig. 9) show a 175-m-thick, deep secondary thermostad in November 1989 between 450 and 625 m. This is much deeper than the lower boundary of the main thermostad of Cyprus Eddy, which is 450 m. To complicate the picture, Brenner et al. (1991) and Brenner (1993) mentioned a possibility (even inevitability) of lateral exchange with ambient waters along isopycnals, the only mechanism that could explain the observed sudden change in  $T$  and  $S$  in the lower layers of thermostad. All three mechanisms invoked can be at work regarding the thermostad, namely successive winter convective events, bottom erosion, and lateral exchange. After all, these mechanisms are not mutually exclusive.

#### (vii) Meddies

Nof and Dewar (1994, p. 1209) noted that "the eddies formed in the Mediterranean outflow (i.e. Meddies) often occur in a so-called double-core state... that resembles the merged state seen by Cresswell (see e.g., Richardson et al., 1989, p. 378)." Indeed, Meddy 2 in Richardson et al. (1989) had two pycnostads, one between 700 and 900 m, and another between 1150 and 1550 m (Richardson et al. 1989, Fig. 11; station 11, 33°55'N, 24°05'W, 5 November 1985), while Meddy 3 (Richardson et al. 1989, Fig. 16, R/V *Meteor* station 315, 22.00°N, 26.07°W, 12 November 1986) had two temperature and salinity maxima centered at 800 and 1100 m. Yet Richardson et al. (1989, 377–378) noted that the double salinity maxima is "characteristic of Mediterranean Water off Cape St. Vincent (Ambar et al. 1976) which we therefore believe is the likely formation site for Meddy 2." The same conclusion can be made about Meddy 3's likely formation site. Therefore, the double-layer structure of some Meddies is not a result of vertical alignment of two lenses but rather a fingerprint of their formation site stratification. Indeed, the Mediterranean outflow in this area consists of two branches that are well documented (e.g., Ambar et al. 1976). Consequently, some Meddies have two distinct, vertically aligned cores (Richardson et al. 1989; Zenk et al. 1991; Prater and Sanford 1994). The double-core vertical structure can persist for years as the two cores retain their identities within a single eddy despite the eddy drifting several thousand kilometers away from the formation site (Richardson et al. 1989; Zenk et al. 1991).

#### (viii) Arctic Ocean

Dmitrenko et al. (2008) were probably the first to document a double-core eddy in the Arctic Ocean. Their eddy had two vertically aligned cores of Atlantic Water that likely originated in the Fram Strait and Barents Sea inflows separated by a front in the Kara Sea. Zhao and Timmermans (2015) observed several double-core eddies and hypothesized that these eddies originated at a front that separates Eurasian waters from Canadian waters. This boundary, known as the Atlantic–Pacific Water mass front, is aligned with either the Lomonosov Ridge or Alpha–Mendelev Ridge complex (e.g., McLaughlin et al. 1996).

#### (ix) Quasi-stationary anticyclonic eddies

Numerous regions of the World Ocean feature quasi-stationary anticyclonic eddies (QSAEs) that persist for years or decades. Such circulatory features deserve special consideration for at least two reasons. First, such



eddies could undergo more than one winter cooling episode, potentially resulting in double thermostads. Second, such eddies represent a natural trap—or generation site—for lenses. Observations from some QSAEs are already available as reviewed above. Examples of such QSAEs (including retroreflections with QSAE-type circulation inside) are the Agulhas Retroflection, East Australian Current Retroflection, Brazil Current Retroflection, North Brazil Current Retroflection, a QSAE downstream of the Large Meander of the Kuroshio, Northwest Corner of the North Atlantic Current, Lofoten Vortex in the Norwegian Sea, Mann Eddy in the Newfoundland Basin, Ulleung Eddy in the Japan Sea, Alboran Gyre in the western Mediterranean, Cyprus Eddy in the eastern Mediterranean, Tsugaru Gyre east of Japan, and Great Whirl–Socotra Gyre in the Somali Current system in the Indian Ocean. The above circulatory features are anticyclonic. Cyclonic retroreflections, albeit rare, could shed fresh and cold lenses that once injected into a larger eddy would appear as secondary thermostads. This process has been observed in the Oyashio Current Retroflection east of Hokkaido (Itoh and Yasuda 2010) and may be at work elsewhere.

## 7. Conclusions

During the R/V *Endeavor* cruise 578 (19–23 May 2016), a warm ring of the Gulf Stream was surveyed south of Georges Bank with CTD, Deep Blue (900 m) XBTs, shipboard ADCPs (75 kHz), near-surface drifters, and satellite SST imagery. The ring was unusual by having two pycnostads: the upper one at 100–200 m with core  $T = 18.14^{\circ}\text{C}$ ,  $S = 36.52$ ,  $\zeta = -0.65f$ , and the lower one at 250–500 m with core  $T = 16.70^{\circ}\text{C}$ ,  $S = 36.35$  and  $\zeta = -0.77f$ . The radial distribution of swirl velocity in the surface layer ( $\sim 50$  m) exhibited solid body rotation to  $\sim 15$ -km radius, a plateau between 15 and 25 km, a further increase to a maximum of  $1.5\text{ m s}^{-1}$  at  $\sim 50$  km, and a rapid decrease outward. The total geostrophic swirl transport relative to 1500 m was about 27 Sv whereas the directly measured transport was estimated to be close to 36 Sv. The surveyed ring has formed due to the vertical alignment of two previously formed warm-core rings of the Gulf Stream. The first ring pinched off from a Gulf Stream meander originated in February 2016 and moved slowly westward from its formation site near  $62^{\circ}\text{W}$ . In April 2016, a second warm-core ring was spawned by a Gulf Stream meander near  $62^{\circ}\text{W}$ , moved rapidly to the west, caught up with the first ring, and coalesced with it at  $64^{\circ}\text{W}$  to form the observed double-thermostad ring. Extensive use of satellite data (high-resolution SST images and daily SSH maps), combined

with in situ observations (XBT/CTD/ADCP/near-surface drifters), allowed the entire life history of this ring to be reconstructed. This fortuitous set of observations allowed the first description of a double-thermostad warm-core ring of the Gulf Stream in the Slope Sea and comprised one of the best-documented cases of vertical alignment of two eddies in the World Ocean.

*Acknowledgments.* The Captain and crew of R/V *Endeavor* greatly contributed to the success of the cruise. We express our sincere thanks to the Rhode Island Endeavor Program (RIEP) who provided the funding for the cruise that made this research possible. The Rhode Island Sea Grant Program (RISG) provided the funding for the construction and tracking of surface drifters. Participants in the Rhode Island Teachers at Sea program were very helpful watch standers and assisted with the deployment of the surface drifters. High-resolution AVHRR SST images from NOAA satellites were downloaded from the Rutgers University Coastal Ocean Observation Lab's Web site ([https://marine.rutgers.edu/cool/sat\\_data](https://marine.rutgers.edu/cool/sat_data)) and Johns Hopkins University Applied Physics Laboratory Space Department Ocean Remote Sensing Group's website (<http://fermi.jhuapl.edu/>). Satellite altimeter SSH data were provided by Ssalto/Duacs, CLS Space Oceanography Division, Copernicus Marine and Environment Monitoring Service, and AVISO (<http://www.aviso.altimetry.fr>). I.B. was supported by the Zhejiang Ocean University. A.F. was supported by the Centre for Southern Hemisphere Oceans Research (CSHOR), a partnership between the Commonwealth Scientific and Industrial Research Organisation (CSIRO) and the Qingdao National Laboratory for Marine Science and Technology (QNLN). The original manuscript was improved thanks to insightful comments by two anonymous reviewers, Editor Joseph LaCasce, Mikhail Sokolovskiy, and Georgi Sutyrin.

## REFERENCES

- Ambar, I., M. R. Howe, and M. I. Abdullah, 1976: A physical and chemical description of the Mediterranean outflow in the Gulf of Cadiz. *Dtsch. Hydrogr. Z.*, **29**, 58–68, <https://doi.org/10.1007/BF02227031>.
- Auer, S. J., 1987: Five-year climatological survey of the Gulf Stream system and its associated rings. *J. Geophys. Res.*, **92**, 11 709–11 726, <https://doi.org/10.1029/JC092iC11p11709>.
- Baird, M. E., and K. R. Ridgway, 2012: The southward transport of sub-mesoscale lenses of Bass Strait Water in the centre of anticyclonic mesoscale eddies. *Geophys. Res. Lett.*, **39**, L02603, <https://doi.org/10.1029/2011GL050643>.
- , and Coauthors, 2011: The effect of surface flooding on the physical-biogeochemical dynamics of a warm-core eddy off

- southeast Australia. *Deep-Sea Res. II*, **58**, 592–605, <https://doi.org/10.1016/j.dsr2.2010.10.002>.
- Barceló-Llull, B., and Coauthors, 2017: Anatomy of a subtropical intrathermocline eddy. *Deep-Sea Res. I*, **124**, 126–139, <https://doi.org/10.1016/j.dsr.2017.03.012>.
- Belkin, I. M., and Yu. G. Mikhailichenko, 1986: Thermohaline structure of the northwest Pacific frontal zone near 160°E. *Oceanology*, **26**, 47–49.
- , and A. L. Gordon, 1996: Southern Ocean fronts from the Greenwich meridian to Tasmania. *J. Geophys. Res.*, **101**, 3675–3696, <https://doi.org/10.1029/95JC02750>.
- , M. V. Emelianov, A. G. Kostianoy, and K. N. Fedorov, 1986: Thermohaline structure of intermediate waters of the ocean and intrathermocline eddies (in Russian). *Intrathermocline Eddies in the Ocean*, K. N. Fedorov, Ed., Shirshov Institute of Oceanology, 8–34.
- Bogdanov, K. T., V. I. Il'ichev, V. B. Lobanov, and R. D. Medzhitov, 1985: An anticyclonic eddy in the northwestern Pacific. *Doklady Akademii Nauk SSSR*, **281**, 202–204.
- Brenner, S., 1993: Long-term evolution and dynamics of a persistent warm core eddy in the Eastern Mediterranean Sea. *Deep-Sea Res. II*, **40**, 1193–1206, [https://doi.org/10.1016/0967-0645\(93\)90067-W](https://doi.org/10.1016/0967-0645(93)90067-W).
- , Z. Rozenraub, J. Bishop, and M. Krom, 1991: The mixed-layer/thermocline cycle of a persistent warm core eddy in the Eastern Mediterranean. *Dyn. Atmos. Oceans*, **15**, 457–476, [https://doi.org/10.1016/0377-0265\(91\)90028-E](https://doi.org/10.1016/0377-0265(91)90028-E).
- Brundage, W. L., and J. P. Dugan, 1986: Observations of an anticyclonic eddy of 18°C water in the Sargasso Sea. *J. Phys. Oceanogr.*, **16**, 717–727, [https://doi.org/10.1175/1520-0485\(1986\)016<0717:OOAAEO>2.0.CO;2](https://doi.org/10.1175/1520-0485(1986)016<0717:OOAAEO>2.0.CO;2).
- Carton, X., 2001: Hydrodynamical modeling of oceanic vortices. *Surv. Geophys.*, **22**, 179–263, <https://doi.org/10.1023/A:1013779219578>.
- Cerone, J. F., 1984: Satellite observed climatology of warm core Gulf Stream rings and discussion of their possible biological effects. M.S. thesis, Graduate School of Oceanography, University of Rhode Island, 179 pp.
- Chapman, P., and D. Nof, 1988: The sinking of warm-core rings. *J. Phys. Oceanogr.*, **18**, 565–583, [https://doi.org/10.1175/1520-0485\(1988\)018<0565:TSOWCR>2.0.CO;2](https://doi.org/10.1175/1520-0485(1988)018<0565:TSOWCR>2.0.CO;2).
- Cook, S. K., 1979: Water column thermal structure across the shelf and slope southeast of Sandy Hook, New Jersey, USA, in 1977. *Ann. Biol.*, **34**, 14–21.
- , 1985: Water column thermal structure across the shelf and slope southeast of Sandy Hook, New Jersey, in 1982. *Ann. Biol.*, **39**, 14–16.
- Cresswell, G. R., 1982: The coalescence of two East Australian current warm-core eddies. *Science*, **215**, 161–164, <https://doi.org/10.1126/science.215.4529.161>.
- , 1983: Physical evolution of Tasman Sea eddy J. *Aust. J. Mar. Freshwater Res.*, **34**, 495–513, <https://doi.org/10.1071/MF9830495>.
- , and R. Legeckis, 1986: Eddies off southeastern Australia. *Deep-Sea Res.*, **33A**, 1527–1562, [https://doi.org/10.1016/0198-0149\(86\)90066-X](https://doi.org/10.1016/0198-0149(86)90066-X).
- Csanady, G. T., and P. Hamilton, 1988: Circulation of slope-water. *Cont. Shelf Res.*, **8**, 565–624, [https://doi.org/10.1016/0278-4343\(88\)90068-4](https://doi.org/10.1016/0278-4343(88)90068-4).
- Dewar, W. K., 1986: Mixed layers in Gulf Stream rings. *Dyn. Atmos. Oceans*, **10**, 1–29, [https://doi.org/10.1016/0377-0265\(86\)90007-2](https://doi.org/10.1016/0377-0265(86)90007-2).
- Dmitrenko, I. A., S. A. Kirillov, V. V. Ivanov, and R. A. Woodgate, 2008: Mesoscale Atlantic water eddy off the Laptev Sea continental slope carries the signature of upstream interaction. *J. Geophys. Res.*, **113**, C07005, <https://doi.org/10.1029/2007JC004491>.
- Dugan, J. P., R. R. Mied, P. C. Mignerey, and A. F. Schuetz, 1982: Compact, intrathermocline eddies in the Sargasso Sea. *J. Geophys. Res.*, **87**, 385–393, <https://doi.org/10.1029/JC087iC01p00385>.
- Fitzgerald, J. L., and J. L. Chamberlin, 1984: Anticyclonic warm-core Gulf Stream rings off the northeastern United States in 1981. *Ann. Biol.*, **38**, 29–33.
- Fofonoff, N. P., 1962: Dynamics of ocean currents. *Physical Oceanography*, M. N. Hill, Ed., *The Sea—Ideas and Observations on Progress in the Study of the Seas*, Vol. 1, Wiley-Interscience, 323–395.
- Gordon, A. L., J. R. E. Lutjeharms, and M. L. Gründlingh, 1987: Stratification and circulation at the Agulhas Retroflection. *Deep-Sea Res.*, **34A**, 565–599, [https://doi.org/10.1016/0198-0149\(87\)90006-9](https://doi.org/10.1016/0198-0149(87)90006-9).
- Hallock, Z. R., W. J. Teague, and R. D. Broome, 1981: A deep, thick, isopycnal layer within an anticyclonic eddy. *J. Phys. Oceanogr.*, **11**, 1674–1677, [https://doi.org/10.1175/1520-0485\(1981\)011<1674:ADTILW>2.0.CO;2](https://doi.org/10.1175/1520-0485(1981)011<1674:ADTILW>2.0.CO;2).
- Hughes, M. M., and S. K. Cook, 1983: Water column thermal structure across the shelf and slope southeast of Sandy Hook, New Jersey, in 1980. *Ann. Biol.*, **37**, 14–18.
- Hummon, J., and T. Rossby, 1998: Spatial and temporal evolution of a Gulf Stream crest-warm core ring interaction. *J. Geophys. Res.*, **103**, 2795–2809, <https://doi.org/10.1029/97JC02375>.
- Itoh, S., and I. Yasuda, 2010: Water mass structure of warm and cold anticyclonic eddies in the western boundary region of the subarctic North Pacific. *J. Phys. Oceanogr.*, **40**, 2624–2642, <https://doi.org/10.1175/2010JPO4475.1>.
- , Y. Shimizu, S. Ito, and I. Yasuda, 2011: Evolution and decay of a warm-core ring within the western subarctic gyre of the North Pacific, as observed by profiling floats. *J. Oceanogr.*, **67**, 281–293, <https://doi.org/10.1007/s10872-011-0027-2>.
- Kaneko, H., S. Itoh, S. Kouketsu, T. Okunishi, S. Hosoda, and T. Suga, 2015: Evolution and modulation of a poleward-propagating anticyclonic eddy along the Japan and Kuril-Kamchatka trenches. *J. Geophys. Res. Oceans*, **120**, 4418–4440, <https://doi.org/10.1002/2014JC010693>.
- Kostianoy, A. G., and I. M. Belkin, 1989: A survey of observations on intrathermocline eddies in the World Ocean. *Mesoscale/Synoptic Coherent Structures in Geophysical Turbulence*, J. C. J. Nihoul and B. M. Jamart, Eds., Elsevier, 821–841.
- Krom, M. D., S. Brenner, N. Kress, A. Neori, and L. I. Gordon, 1992: Nutrient dynamics and new production in a warm-core eddy from the Eastern Mediterranean Sea. *Deep-Sea Res.*, **39A**, 467–480, [https://doi.org/10.1016/0198-0149\(92\)90083-6](https://doi.org/10.1016/0198-0149(92)90083-6).
- , —, —, —, and —, 1993: Nutrient distributions during an annual cycle across a warm core eddy from the E. Mediterranean Sea. *Deep-Sea Res. I*, **40**, 805–825, [https://doi.org/10.1016/0967-0637\(93\)90073-C](https://doi.org/10.1016/0967-0637(93)90073-C).
- Leavitt, D., and Coauthors, 2015: An assessment of quahog larval supply and distribution in the upper Narragansett Bay with a focus on spawning sanctuaries and alternative area management strategies. Appendix M in Southern New England Collaborative Research Initiative Final Report, Commercial Fisheries Research Foundation, 63 pp., <http://www.cfrfoundation.org/quahog-larval-supply-assessment>.
- Leetmaa, A., 1976: Recent observations of eddies south-west of Bermuda. *POLYMODE News*, No. 10, Woods Hole

- Oceanographic Institution, Woods Hole, MA, 1–5, <http://darchive.mblwhoilibrary.org/bitstream/handle/1912/8120/10.pdf>.
- Lilly, J. M., and Coauthors, 2003: Observations of the Labrador Sea eddy field. *Prog. Oceanogr.*, **59**, 75–176, <https://doi.org/10.1016/j.pocean.2003.08.013>.
- Macdonald, H. S., M. Roughtan, M. E. Baird, and J. Wilkin, 2013: A numerical modeling study of the East Australian Current encircling and overwashing a warm-core eddy. *J. Geophys. Res. Oceans*, **118**, 301–315, <https://doi.org/10.1029/2012JC008386>.
- Manning, J. P., D. J. McGillicuddy Jr., N. R. Pettigrew, J. H. Churchill, and L. S. Incze, 2009: Drifter observations of the Gulf of Maine Coastal Current. *Cont. Shelf Res.*, **29**, 835–845, <https://doi.org/10.1016/j.csr.2008.12.008>.
- McCartney, M. S., and M. E. Woodgate-Jones, 1991: A deep-reaching anticyclonic eddy in the subtropical gyre of the eastern South Atlantic. *Deep-Sea Res.*, **38A**, S411–S443, [https://doi.org/10.1016/S0198-0149\(12\)80019-7](https://doi.org/10.1016/S0198-0149(12)80019-7).
- McLaughlin, F. A., E. C. Carmack, R. W. Macdonald, and J. K. B. Bishop, 1996: Physical and geochemical properties across the Atlantic/Pacific water mass front in the southern Canadian Basin. *J. Geophys. Res.*, **101**, 1183–1197, <https://doi.org/10.1029/95JC02634>.
- McWilliams, J. C., 1985: Submesoscale, coherent vortices in the ocean. *Rev. Geophys.*, **23**, 165–182, <https://doi.org/10.1029/RG023i002p00165>.
- , 2016: Submesoscale currents in the ocean. *Proc. Roy. Soc. London A*, **472**, 20160117, <https://doi.org/10.1098/rspa.2016.0117>.
- Monim, M., 2017: Seasonal and inter-annual variability of the Gulf Stream warm core rings from 2000 to 2016. M.S. thesis, School for Marine Science and Technology, University of Massachusetts Dartmouth, 123 pp.
- Nilsson, C. S., and G. R. Cresswell, 1980: The formation and evolution of East Australian current warm-core eddies. *Prog. Oceanogr.*, **9**, 133–183, [https://doi.org/10.1016/0079-6611\(80\)90008-7](https://doi.org/10.1016/0079-6611(80)90008-7).
- Nof, D., and W. K. Dewar, 1994: Alignment of lenses: Laboratory and numerical experiments. *Deep-Sea Res. I*, **41**, 1207–1229, [https://doi.org/10.1016/0967-0637\(94\)90041-8](https://doi.org/10.1016/0967-0637(94)90041-8).
- Olson, D. B., 1991: Rings in the ocean. *Annu. Rev. Earth Planet. Sci.*, **19**, 283–311, <https://doi.org/10.1146/annurev.ea.19.050191.001435>.
- , R. A. Fine, and A. L. Gordon, 1992: Convective modifications of water masses in the Agulhas. *Deep-Sea Res.*, **39A**, S163–S181, [https://doi.org/10.1016/S0198-0149\(11\)80010-5](https://doi.org/10.1016/S0198-0149(11)80010-5).
- Polvani, L. M., 1991: Two-layer geostrophic vortex dynamics. Part 2. Alignment and two-layer V-states. *J. Fluid Mech.*, **225**, 241–270, <https://doi.org/10.1017/S0022112091002045>.
- Prater, M. D., and T. B. Sanford, 1994: A meddy off Cape St. Vincent. Part I: Description. *J. Phys. Oceanogr.*, **24**, 1572–1586, [https://doi.org/10.1175/1520-0485\(1994\)024<1572:AMOCSV>2.0.CO;2](https://doi.org/10.1175/1520-0485(1994)024<1572:AMOCSV>2.0.CO;2).
- Richardson, P. L., 1980: Gulf Stream ring trajectories. *J. Phys. Oceanogr.*, **10**, 90–104, [https://doi.org/10.1175/1520-0485\(1980\)010<0090:GSRT>2.0.CO;2](https://doi.org/10.1175/1520-0485(1980)010<0090:GSRT>2.0.CO;2).
- , D. Walsh, L. Armi, M. Schröder, and J. F. Price, 1989: Tracking three meddies with SOFAR floats. *J. Phys. Oceanogr.*, **19**, 371–383, [https://doi.org/10.1175/1520-0485\(1989\)019<0371:TTMWSF>2.0.CO;2](https://doi.org/10.1175/1520-0485(1989)019<0371:TTMWSF>2.0.CO;2).
- Rogachev, K., N. Shlyk, and E. Carmack, 2007: The shedding of mesoscale anticyclonic eddies from the Alaskan Stream and westward transport of warm water. *Deep-Sea Res. II*, **54**, 2643–2656, <https://doi.org/10.1016/j.dsr2.2007.08.017>.
- Rossby, T., 2014: On the structure and distribution of thin anticyclonic lenses in the southeast Pacific Ocean. *J. Mar. Res.*, **72**, 383–403, <https://doi.org/10.1357/002224014815540651>.
- , C. Flagg, P. Ortner, and C. Hu, 2011: A tale of two eddies: Diagnosing coherent eddies through acoustic remote sensing. *J. Geophys. Res.*, **116**, C12017, <https://doi.org/10.1029/2011JC007307>.
- Schmitt, R. W., and D. B. Olson, 1985: Wintertime convection in warm-core rings: Thermocline ventilation and the formation of mesoscale lenses. *J. Geophys. Res.*, **90**, 8823–8837, <https://doi.org/10.1029/JC090iC05p08823>.
- Sokolovskiy, M. A., and J. Verron, 2014: *Dynamics of Vortex Structures in a Stratified Rotating Fluid*. Springer, 382 pp.
- Stammer, D., and J. Theiss, 2004: Velocity statistics inferred from the TOPEX/Poseidon-Jason-1 Tandem mission data. *Mar. Geod.*, **27**, 551–575, <https://doi.org/10.1080/01490410490902052>.
- Tomosada, A., 1978: A large warm eddy detached from the Kuroshio east of Japan. *Bull. Tokai Reg. Fish. Res. Lab.*, **94**, 59–103.
- van Aken, H. M., and Coauthors, 2003: Observations of a young Agulhas ring, Astrid, during MARE in March 2000. *Deep-Sea Res. II*, **50**, 167–195, [https://doi.org/10.1016/S0967-0645\(02\)00383-1](https://doi.org/10.1016/S0967-0645(02)00383-1).
- Zantopp, R., and K. Leaman, 1982: Gulf of Cadiz water observed in a thermocline eddy in the western North Atlantic. *J. Geophys. Res.*, **87**, 1927–1934, <https://doi.org/10.1029/JC087iC03p01927>.
- Zenk, W., B. Klein, and M. Schröder, 1991: Cape Verde Frontal Zone. *Deep-Sea Res.*, **38A**, S505–S530, [https://doi.org/10.1016/S0198-0149\(12\)80022-7](https://doi.org/10.1016/S0198-0149(12)80022-7).
- Zhao, M., and M.-L. Timmermans, 2015: Vertical scales and dynamics of eddies in the Arctic Ocean's Canada Basin. *J. Geophys. Res. Oceans*, **120**, 8195–8209, <https://doi.org/10.1002/2015JC011251>.